Magnetic structures and physical properties of $Tm_3Cu_4Ge_4$ and $Tm_3Cu_4Sn_4$

2013 J. Phys.: Condens. Matter 25 066012

(http://iopscience.iop.org/0953-8984/25/6/066012)

J. Phys.: Condens. Matter **25** (2013) 066012 (9pp) doi:10.1088/0953-8984/25/6/066012

Magnetic structures and physical properties of $Tm_3Cu_4Ge_4$ and $Tm_3Cu_4Sn_4$

S Baran[1], D Kaczorowski[2], A Szytuła[1], A Gil[3] and A Hoser[4]

[1] M Smoluchowski Institute of Physics, Jagiellonian University, Reymonta 4, PL-30 059 Kraków, Poland
[2] Institute of Low Temperature and Structure Research, Polish Academy of Sciences, PO Box 1410, PL-50 950 Wrocław, Poland
[3] Faculty of Mathematical and Natural Sciences, Jan Długosz University in Częstchowa, Aleja Armii Krajowej 13/15, Częstochowa PL-42 200, Poland
[4] Helmholtz-Zentrum Berlin für Materialien und Energie GmbH, Hahn-Meitner Platz 1, D-14 109 Berlin, Germany

E-mail: stanislaw.baran@uj.edu.pl

Received 3 October 2012, in final form 21 December 2012
Published 18 January 2013
Online at stacks.iop.org/JPhysCM/25/066012

Abstract

$Tm_3Cu_4Ge_4$ crystallizes in the orthorhombic $Gd_3Cu_4Ge_4$-type crystal structure (space group *Immm*) whereas $Tm_3Cu_4Sn_4$ crystallizes in a distorted variant of this structure (monoclinic space group $C2/m$). The compounds were studied by means of neutron diffraction, specific heat, electrical resistivity and magnetic measurements. Analysis of experimental data revealed the presence of an antiferromagnetic order below 2.8 K in both compounds. In $Tm_3Cu_4Ge_4$ the magnetic unit cell is doubled in respect to the crystal unit cell and the magnetic structure can be described by a propagation vector $\vec{k} = [0, \frac{1}{2}, 0]$. A larger magnetic unit cell was found in $Tm_3Cu_4Sn_4$, given by a propagation vector $\vec{k} = [\frac{1}{2}, \frac{1}{2}, 0]$ (for simplicity the orthorhombic description is used for both the germanide and the stannide). Close to 2 K, in each compound an incommensurate antiferromagnetic order develops. This low-temperature magnetic phase is characterized by a propagation vector $\vec{k} = [\frac{1}{4}, 0, k_z]$, where k_z is close to 0.49 and 0.47 in $Tm_3Cu_4Ge_4$ and $Tm_3Cu_4Sn_4$, respectively. The antiferromagnetic phase transitions are clearly seen in the bulk magnetic and specific heat data of both compounds.

1. Introduction

The ternary intermetallics $R_3Cu_4X_4$ (R = rare earth element; X = Ge, Sn) have been intensively investigated for the past decade due to their intriguing physical properties [1, 2]. Most of these compounds crystallize in an orthorhombic structure of the $Gd_3Cu_4Ge_4$-type (space group *Immm*, #71) [3]; however the stannides $R_3Cu_4Sn_4$ (R = Tm and Lu) form with a monoclinic structure (space group $C2/m$, #12) at room temperature [4, 5], which is a distorted variant of the orthorhombic one. In recent studies, $Ho_3Cu_4Sn_4$ and $Er_3Cu_4Sn_4$ were found to change their orthorhombic crystal structure to a monoclinic structure characterized by the space group $I2/m$ upon cooling at 62 K and 262 K, respectively [7]. In turn, $Tm_3Cu_4Sn_4$ was reported to undergo a transition from its monoclinic unit cell to an orthorhombic cell of the *Immm* space symmetry at 458 K upon heating [6].

In general, those $R_3Cu_4X_4$ intermetallics which were found to order magnetically at low temperatures have an antiferromagnetic spin arrangement, except for $Yb_3Cu_4Ge_4$, which is a ferromagnet below 7.5 K [8]. $La_3Cu_4Sn_4$ is diamagnetic down to 1.5 K [9]. The heavy-fermion compound $Ce_3Cu_4Ge_4$ orders antiferromagnetically at the Néel temperature of 10.3 K and undergoes two subsequent magnetic phase transitions at 7.8 and 2.6 K [1]. Similar behavior was reported for $Ce_3Cu_4Sn_4$, with the corresponding temperatures equal to 10.3, 7.3 and 2.6 K [1]. $Pr_3Cu_4Sn_4$ has a Néel point of about 11 K [9, 10]. The germanide $Nd_3Cu_4Ge_4$

orders at 4.5 K [11], while the ordering temperature for the Nd-based stannide was reported to be between 1.8 K [9] and 2.0 K [2, 12]. The postulated magnetic ordering in $Nd_3Cu_4Sn_4$ was however not confirmed in neutron diffraction experiments performed down to 1.5 K [10]. Similarly, multiple magnetic transitions were observed in $Sm_3Cu_4Sn_4$, namely at 9, 7.5 and 5 K [9], while more recent neutron diffraction studies reported no long-range magnetic ordering down to 3 K [2]. For $Gd_3Cu_4Ge_4$, the following magnetic ordering temperatures were reported: 8.6 K [8], 16 K [13, 14] and 11 K [15]. For the corresponding stannide $Gd_3Cu_4Sn_4$ the reported Néel temperatures are: 13 K [15, 16], 13.6 K [17] and 14 K [13, 14]. Moreover, an additional order–order magnetic transition was reported to occur at 8.6 K [16] for this compound. In $Tb_3Cu_4Ge_4$, the Tb magnetic moments located at the 2d site order magnetically at $T_N(2d) = 23$ K and then undergo another magnetic transition at $T_t = 18$ K, while the Tb moments at the 4e site order at $T_N(4e) = 10$ K [13, 14, 18]. The $R_3Cu_4Sn_4$ (R = Tb, Dy) stannides become antiferromagnetic below about 17.5 K and 15 K for R = Tb and Dy, respectively [13, 14, 19]. In turn, Néel temperatures of 16.2 and 9.5 K were reported for the corresponding germanides, i.e., $Dy_3Cu_4Ge_4$ and $Ho_3Cu_4Ge_4$, respectively [13, 14, 18]. A complex magnetic ordering was found in $Ho_3Cu_4Sn_4$. In this compound the magnetic moments located at the 2d sublattice order at the Néel point of about 8 K, while those located at the 4e sublattice order at about 3 K. Below the Néel point a number of magnetic transitions related to reorientation of the magnetic moments and/or change of magnetic propagation vector were observed [12–14, 19, 21]. The Néel temperatures reported for $Er_3Cu_4Ge_4$ are between 7.6 and 7.9 K for the 2d sublattice and about 3 K for the 4e sublattice. An incommensurate magnetic order was found to develop between 7 and 7.6 K [13, 14, 18, 22]. The most recent studies evidenced an order–order magnetic phase transition in the 4e sublattice at 1.4 K [20]. In $Er_3Cu_4Sn_4$, the 2d sublattice orders at about 6 K, while the ordering temperature of the 4e sublattice was estimated to be between 2 and 3 K [13, 14, 19]. However, the Mössbauer spectroscopy data show no long-range magnetic ordering in the 4e sublattice down to 2 K [22], in line with the results of neutron diffraction experiments [13, 14, 19].

In this paper we report on the magnetic behavior in $Tm_3Cu_4X_4$ (X = Ge, Sn) studied by means of magnetic susceptibility, magnetization, electrical resistivity and heat capacity measurements. The magnetic structures of these compounds were investigated by powder neutron diffraction.

2. Experimental details

Polycrystalline samples of $Tm_3Cu_4X_4$ (X = Ge, Sn) were synthesized by arc melting high-purity elements (3N for Tm; 4N for Cu, Ge and Sn) under argon atmosphere. The ingots were turned over and remelted several times to ensure sample homogeneity. Afterwards, they were sealed in evacuated quartz capsules and annealed at 600 °C for one week. The quality of the products was examined by means of powder x-ray diffraction using a Philips PW-3710 X'PERT diffractometer equipped with a copper anode.

Magnetic susceptibility measurements were carried out over the temperature interval 1.72–400 K in an applied magnetic field of 0.1 T, while the isothermal magnetization data were collected at 1.72 K in external magnetic fields up to 5 T. These measurements were performed using a Quantum Design SQUID magnetometer. The heat capacity was investigated by a relaxation method in the temperature range 0.5–300 K by employing using a Quantum Design PPMS platform. Electrical resistivity measurements were carried out over the temperature interval 0.4–300 K using a Quantum Design PPMS platform.

The crystal and magnetic structures were examined by neutron powder diffraction. The neutron data were collected over the temperature interval from 1.5 K up to 4.9 K using the E6 diffractometer installed at the BERII reactor (Helmholtz-Zentrum Berlin). The incident neutron wavelength was 2.447 Å. The obtained diffraction data were analyzed using the Rietveld-type program FullProf [23].

3. Crystal structure

The x-ray diffraction experiment performed at room temperature and the neutron diffraction experiment done at 4.9 K (at this temperature both investigated compounds are still in the paramagnetic state) confirmed the crystal structures reported in the literature, namely the orthorhombic $Gd_3Cu_4Ge_4$-type (space group *Immm*) unit cell for $Tm_3Cu_4Ge_4$ and the monoclinic (space group $C2/m$) unit cell for $Tm_3Cu_4Sn_4$. Table 1 contains information on the crystal structures derived from the neutron diffraction data. As a representative of the collected diffraction patterns and their analyses, figure 1 shows the neutron result obtained for the germanide.

Six thulium atoms in $Tm_3Cu_4Ge_4$ and $Tm_3Cu_4Sn_4$ occupy two different Wyckoff positions: 2d and 4e in the orthorhombic unit cell of the germanide, and 2c and 4i in the monoclinic unit cell of the stannide (table 2).

4. Magnetic behavior

Figure 2 shows the temperature dependences of the reciprocal magnetic susceptibility of $Tm_3Cu_4Ge_4$ and $Tm_3Cu_4Sn_4$. At high enough temperatures (above 100 K), the susceptibility of both compounds obeys a Curie–Weiss (CW) law. At low temperatures some deviation from a straight-line behavior is observed (especially for the germanide), which likely signals crystalline electric field (CEF) interactions. The CW fits to the experimental data yielded an effective magnetic moment of 7.35 μ_B and 7.44 μ_B for the germanide and the stannide, respectively. These values are close to those predicted within a Russell–Saunders coupling scenario for a free Tm^{3+} ion (7.56 μ_B). The paramagnetic Curie temperatures obtained for the CW fits are equal to 5.0 K and −4.6 K for $Tm_3Cu_4Ge_4$ and $Tm_3Cu_4Sn_4$, respectively. The opposite signs of θ_p hint at different dominant character of the magnetic exchange interactions in these two compounds, which in consequence leads to their different magnetic structures (see below).

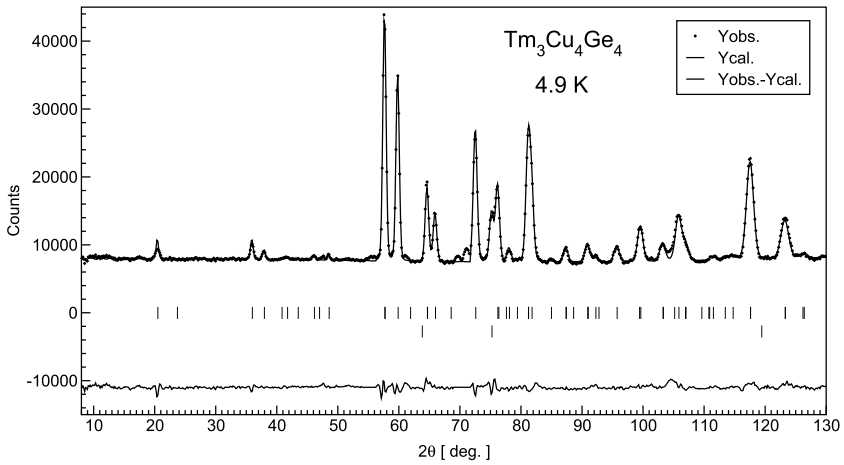

Figure 1. Neutron diffraction pattern of $Tm_3Cu_4Ge_4$ collected at 4.9 K together with the Rietveld fit and difference plot. The upper row of vertical ticks indicates the positions of $Tm_3Cu_4Ge_4$ nuclear Bragg reflections while the second row indicates the reflections originating from aluminum cryostat shielding. The small peaks at 61.0°, 69.7° and 71.1° come from an unidentified impurity. The regions containing impurity reflections were excluded from refinement.

Table 1. Crystal structure parameters of $Tm_3Cu_4X_4$ (X = Ge, Sn) together with residuals for profile and integrated intensities. The parameters were derived from paramagnetic neutron diffraction patterns collected at 4.9 K. WP denotes Wyckoff position.

Compound	$Tm_3Cu_4Ge_4$			$Tm_3Cu_4Sn_4$		
Crystal system	Orthorhombic			Monoclinic		
Space group	*Immm*			*C*2/*m*		
Space group no.	71			12		
	Atom	WP	Coordinates	Atom	WP	Coordinates
	Tm_1	2d	$0, \frac{1}{2}, 0$	Tm_1	2c	$0, 0, \frac{1}{2}$
	Tm_2	4e	0.1299(12), 0, 0	Tm_2	4i	0.1301(17), 0, 0.1205(48)
	Cu	8n	0.3297(7), 0.1917(14), 0	Cu_1	4i	0.3177(18), 0, 0.5137(45)
	Ge_1	4f	0.2174(10), $\frac{1}{2}$, 0	Cu_2	4i	0.3397(15), 0, 0.1533(40)
	Ge_2	4h	$0, 0.1895(19), \frac{1}{2}$	Sn_1	4i	0.2151(18), 0, 0.7307(64)
				Sn_2	4i	0.5104(20), 0, 0.2019(46)
a (Å)	13.7176(14)			16.0856(34)		
b (Å)	6.5964(8)			4.3838(8)		
c (Å)	4.1321(4)			6.8855(16)		
α, β, γ (deg)	90, 90, 90			90, 115.982(14), 90		
V (Å^3)	373.90(7)			436.46(17)		
$R_{profile}$ (%)	2.20			2.43		
R_{Bragg} (%)	5.18			5.28		

Table 2. Coordinates of six thulium atoms in elementary unit cell. The values of refined positional parameters should be taken from table 1. WP denotes Wyckoff position.

Compound	$Tm_3Cu_4Ge_4$		$Tm_3Cu_4Sn_4$	
Crystal system	Orthorhombic		Monoclinic	
Space group	*Immm*		*C*2/*m*	
Space group no.	71		12	
Atom	WP	Coordinates	WP	Coordinates
Tm_{11}	2d	$0, \frac{1}{2}, 0$	2c	$0, 0, \frac{1}{2}$
Tm_{12}	2d	$\frac{1}{2}, 0, \frac{1}{2}$	2c	$\frac{1}{2}, \frac{1}{2}, \frac{1}{2}$
Tm_{21}	4e	$x_{Tm}, 0, 0$	4i	$x_{Tm}, 0, z_{Tm}$
Tm_{22}	4e	$\bar{x}_{Tm}, 0, 0$	4i	$\bar{x}_{Tm}, 0, \bar{z}_{Tm}$
Tm_{23}	4e	$\frac{1}{2} + x_{Tm}, \frac{1}{2}, \frac{1}{2}$	4i	$\frac{1}{2} + x_{Tm}, \frac{1}{2}, z_{Tm}$
Tm_{24}	4e	$\frac{1}{2} - x_{Tm}, \frac{1}{2}, \frac{1}{2}$	4i	$\frac{1}{2} - x_{Tm}, \frac{1}{2}, \bar{z}_{Tm}$

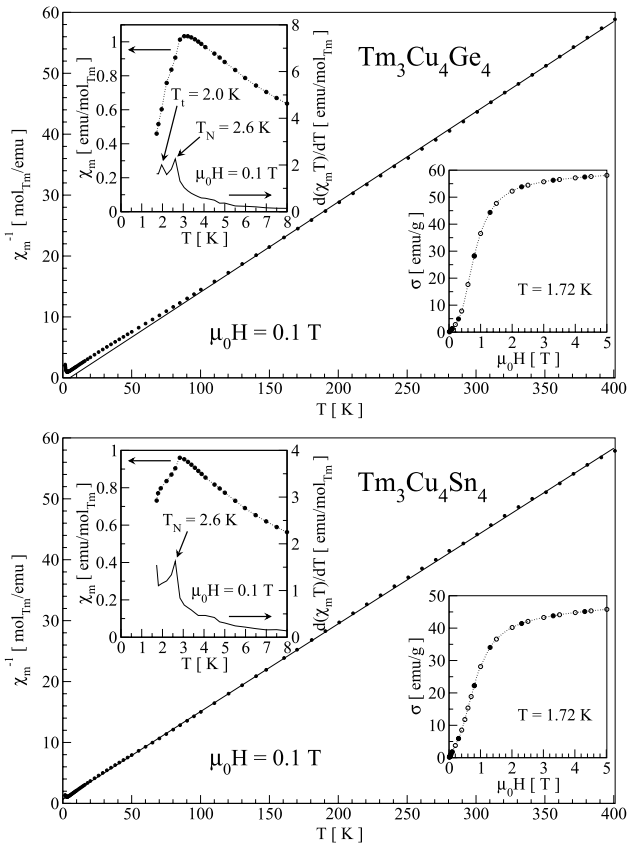

Figure 2. Inverse magnetic susceptibility of $Tm_3Cu_4X_4$ (X = Ge, Sn). The solid lines show the Curie–Weiss fits discussed in the text. The upper-left corner insets present magnetic susceptibility at low temperatures together with the derivative $d(\chi_m T)/dT$. The bottom-right corner insets present isothermal magnetization while increasing (open symbols) and decreasing (filled symbols) the applied magnetic field.

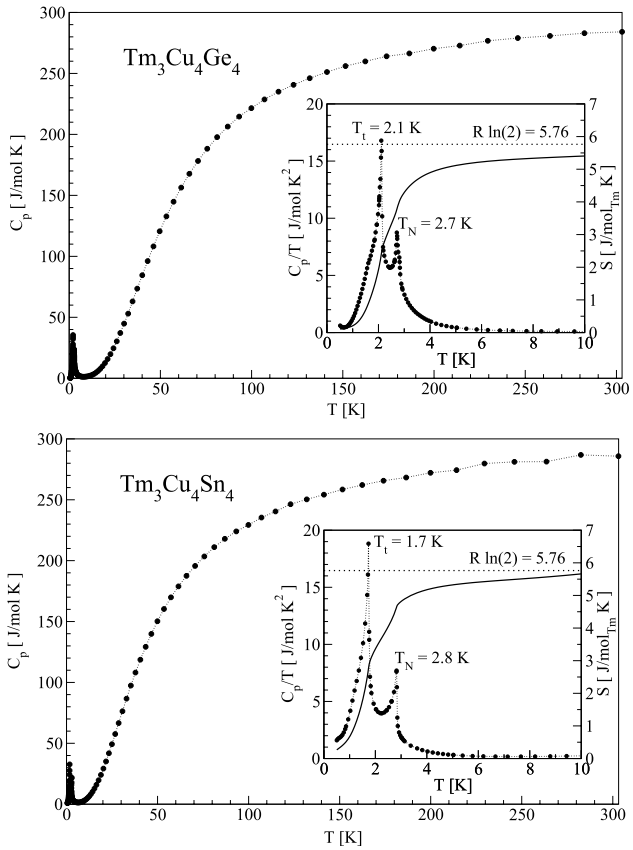

Figure 3. Temperature dependences of the specific heat of $Tm_3Cu_4X_4$ (X = Ge, Sn). The insets present the low-temperature specific heat data in the form of the ratio C/T (dots) and the corresponding entropy (solid line).

As can be inferred from the upper insets in figure 2, the $\chi_m(T)$ functions at low temperatures exhibit maxima characteristic of transitions from the para- to antiferromagnetic state. The Néel temperature estimated from the temperature derivative $d\chi_m/dT$ is equal to 2.6 K for both compounds. In the case of the germanide the derivative shows another maximum at $T_t = 2.0$ K, which might be attributed to an order–order phase transition, while for the stannide a sharp upturn in $d\chi_m/dT$ hints at a similar transition taking place below 1.72 K.

The lower insets in figure 2 display the isothermal magnetization curves, taken at 1.72 K. They exhibit metamagnetic-like inflections at 0.28 T and 0.36 T for the germanide and the stannide, respectively. In strong magnetic fields the magnetization shows a tendency for saturation, which is however not reached up to $\mu_0 H = 5$ T. The magnetic moment per Tm atom attained in this field equals 3.65 μ_B for $Tm_3Cu_4Ge_4$ and 3.38 μ_B for $Tm_3Cu_4Sn_4$. These values are close to half of the theoretical value calculated for a free Tm^{3+} ion (7.0 μ_B). The observed reduction results presumably from the CEF effect.

5. Specific heat

The temperature variations of the specific heat of $Tm_3Cu_4Ge_4$ and $Tm_3Cu_4Sn_4$ are shown in figure 3. They have a usual sigmoid-like shape with the anomalies due to the magnetic phase transitions superimposed. For each compound, the specific heat at room temperature attains a value close to the Dulong–Petit limit. As can be inferred from the insets to figure 3, the lambda-type peak in $C(T)$ occurs for the germanide at 2.7 K and for the stannide at 2.8 K, in good agreement with the Néel temperatures determined from the magnetic susceptibility data. Furthermore, for each compound one observes a much sharper and nearly symmetric peak that signals a first-order transition, likely associated with a change in the magnetic structure. This low-temperature singularity occurs at 2.1 K and 1.7 K for $Tm_3Cu_4Ge_4$ and $Tm_3Cu_4Sn_4$, respectively, and corresponds very well to the findings from the magnetic susceptibility study.

The insets in figure 3 present the temperature evolution of the entropy, calculated from the measured $C/T(T)$ data. Since in the considered temperature region the phonon contribution to the specific heat is negligibly small, it can be assumed that the $S(T)$ functions represent the magnetic entropy in the compounds studied. In each case, above the respective Néel temperature, the entropy reaches a value close to $R\ln(2)$. This

finding indicates a magnetic ground state being a doublet or two singlets closely spaced in energy. These states are probably rather well separated from the rest of the CEF levels resulting from splitting the thulium $^3H_6$ multiplet in the crystal electric field potential of the orthorhombic point symmetry C_{2v} ($mm2$). For detailed analysis of the Schottky contribution to the specific heat of $Tm_3Cu_4Ge_4$ and $Tm_3Cu_4Sn_4$, inelastic neutron diffraction experiments are indispensable.

6. Electrical resistivity

The temperature dependences of the electrical resistivity of $Tm_3Cu_4Ge_4$ and $Tm_3Cu_4Sn_4$ are presented in figure 4. Both compounds exhibit metallic character of the electronic transport. The resistivity decreases almost linearly from room temperature down to about 40 K and 100 K for the germanide and the stannide, respectively, and then shows a tendency to saturate at low temperatures. The latter behavior is interrupted by the onset of the magnetically ordered state, which results in a distinct reduction in the conduction electron scattering on the thulium magnetic moments. The transition temperatures, defined as sharp kinks in $\rho(T)$ (see the insets in figure 4) are 2.8 K for $Tm_3Cu_4Ge_4$ and 2.9 K for $Tm_3Cu_4Sn_4$, in good agreement with the Néel points derived from the other experimental data.

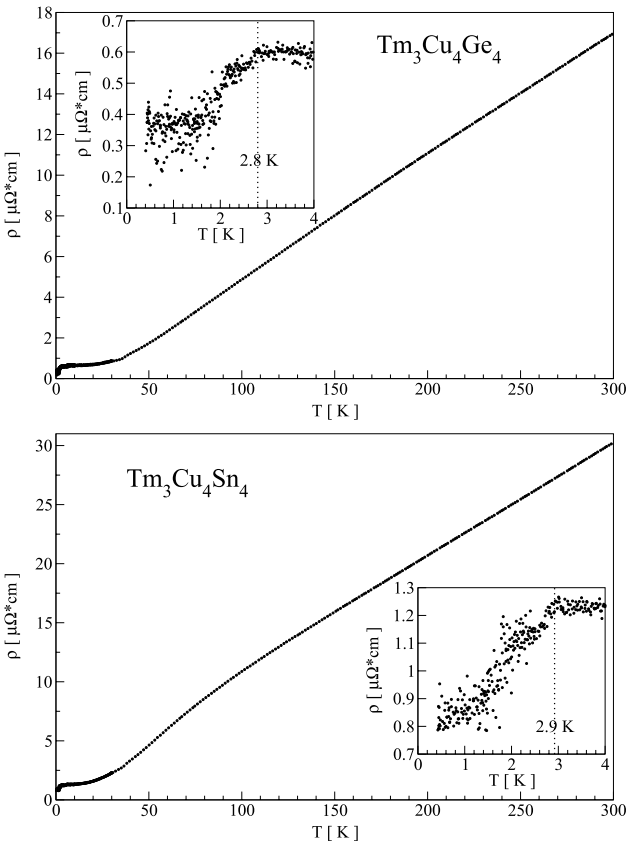

Figure 4. Electrical resistivity of $Tm_3Cu_4X_4$ (X = Ge, Sn). The insets show the low-temperature regime, with vertical lines indicating temperatures at which changes in slope take place.

7. Magnetic structure

For both investigated compounds, a group of Bragg reflections of magnetic origin appears in the neutron diffraction patterns collected at 2.9 K (see the lower parts of figures 5 and 6). These reflections correspond to a commensurate antiferromagnetic order in the 2d thulium sublattice in $Tm_3Cu_4Ge_4$ and the 2c thulium sublattice in $Tm_3Cu_4Sn_4$. The magnetic structure of the germanide may be described by a propagation vector $\vec{k} = [0, \frac{1}{2}, 0]$ with the Tm magnetic moments lying along the crystallographic c-axis. In turn, the propagation vector in $Tm_3Cu_4Sn_4$ equals $\vec{k} = [0, 0, \frac{1}{2}]$ and the Tm magnetic moments are parallel to the b-axis. However, if one neglects a monoclinic distortion in the crystal structure of the stannide and uses the same orthorhombic representation as for $Tm_3Cu_4Ge_4$, then the propagation vector describing the antiferromagnetic structure of $Tm_3Cu_4Sn_4$ may be expressed as $\vec{k}_{ortho} = [\frac{1}{2}, \frac{1}{2}, 0]$ and the magnetic moments are oriented along the c_{ortho}-axis. Within a single crystallographic elementary unit cell the magnetic moments of Tm_{11} and Tm_{12} are coupled ferromagnetically. The commensurate antiferromagnetic structures of both compounds are shown in figure 7, while the results of the magnetic structure refinement are summarized in table 3.

On further decreasing the temperature another group of Bragg reflections develops at 2.3 K and 1.9 K for the germanide and stannide, respectively (see the upper parts of figures 5 and 6). These reflections originate from an incommensurate magnetic structure that involves the 4e thulium sublattice in $Tm_3Cu_4Ge_4$ and the 4i sublattice in $Tm_3Cu_4Sn_4$. The propagation vector equals $\vec{k} = [\frac{1}{4}, 0, k_z]$ in the former compound and $\vec{k} = [\frac{1}{4}, k_y, 0]$ in the latter one, with k_z and k_y being close to 0.5. Actually, this is the same magnetic structure, yet described in a different way. The

Table 3. Refined parameters of $Tm_3Cu_4X_4$ (X = Ge, Sn) commensurate antiferromagnetic order in the 2d (orthorhombic) or 2c (monoclinic) thulium sublattice together with residuals for profile and integrated magnetic intensities. The parameters were derived from the neutron diffraction patterns collected at 2.4 K and 2.0 K for germanide and stannide, respectively. SYM denotes crystal symmetry, PV—propagation vector and DMM—direction of magnetic moment. In case of stannide, for better comparison with the germanide, both the monoclinic and orthorhombic descriptions are presented.

Compound	$Tm_3Cu_4Ge_4$	$Tm_3Cu_4Sn_4$	
T (K)	2.4	2.0	
SYM	Orthorhombic	Monoclinic	Orthorhombic[a]
PV	$[0, \frac{1}{2}, 0]$	$[0, 0, \frac{1}{2}]$	$[\frac{1}{2}, \frac{1}{2}, 0]$
DMM	$\parallel c$	$\parallel b$	$\parallel c_{ortho}$
μ (μ_B)	5.75(23)	5.98(6)	6.17(37)
$R_{magnetic}$ (%)	16.92	9.34	15.09
$R_{profile}$ (%)	1.75	1.43	2.76

[a] In fact the $Tm_3Cu_4Sn_4$ crystal structure shows a monoclinic distortion. The orthorhombic description was only used for easier comparison with $Tm_3Cu_4Ge_4$.

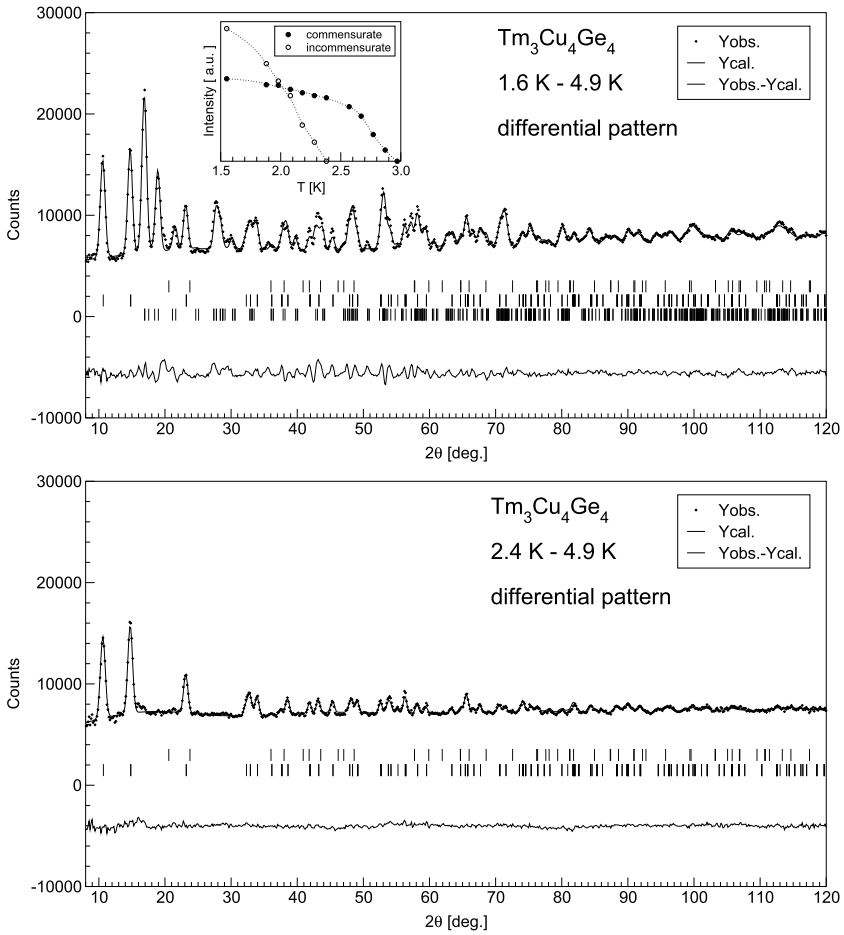

Figure 5. Magnetic contribution to neutron diffraction patterns of $Tm_3Cu_4Ge_4$ collected at 1.6 and 2.4 K together with Rietveld fit and difference plot. The differential patterns were extracted by subtracting the paramagnetic pattern taken at 4.9 K from the low-temperature ones. The upper row of vertical ticks indicates the positions of nuclear reflections (they are absent in differential pattern but were marked as a reference). The next row(s) indicates the positions of reflections originating from magnetic contributions. The inset shows the temperature dependence of magnetic reflections at $2\theta = 10.6°$ and $2\theta = 16.9°$ originating from commensurate and incommensurate magnetic order, respectively.

magnetic moments are parallel to the orthorhombic *b*-axis (or monoclinic *c*-axis). The structure is sine-modulated, which means that the magnetic moment magnitude varies according to the equation:

$$\mu = \mu_A \sin(\vec{k} \cdot \vec{r} + \phi) \quad (1)$$

where μ_A stands for the amplitude of modulation, $\vec{r}$ is a vector pointing from the origin of the coordinate system towards the magnetic atom, and ϕ denotes a phase. Within an elementary unit cell the magnetic moments of Tm_{21} and Tm_{22} are of the same magnitude and are coupled ferromagnetically. The same is true for the pair: Tm_{23} and Tm_{24}. However, there is a phase shift between Tm_{21} (Tm_{22}) and Tm_{23} (Tm_{24}). This phase shift was found to be slightly less than 0.5 (in units of 2π) giving almost antiferromagnetic coupling between Tm_{21} (Tm_{22}) and Tm_{23} (Tm_{24}). The incommensurate component of the magnetic structure is shown in figure 8. The complete description of the low-temperature magnetic structure, which consists of both the commensurate and incommensurate components, is presented in table 4.

8. Conclusions

The diffraction data presented in this paper confirm the orthorhombic crystal structure of $Tm_3Cu_4Ge_4$, and a monoclinic distortion in $Tm_3Cu_4Sn_4$. Both compounds were found to order antiferromagnetically at about 2.8 K and undergo the subsequent magnetic phase transition in the ordered state near 2 K. The characteristic temperatures determined by various methods (magnetic susceptibility, heat capacity, neutron diffraction) are compared in table 5.

The neutron diffraction experiment revealed that in $Tm_3Cu_4Ge_4$ the thulium atoms at the 2d sublattice form at the Néel point a commensurate antiferromagnetic structure with the magnetic moments oriented along the *c*-axis. This magnetic unit cell is presented in figure 7. In $Tm_3Cu_4Sn_4$ the antiferromagnetic commensurate order is quite similar, yet the magnetic unit cell is doubled with respect to that found in the germanide (see figure 7).

With decreasing temperature in the ordered state, the thulium magnetic moments at the 4e sublattice of $Tm_3Cu_4Ge_4$

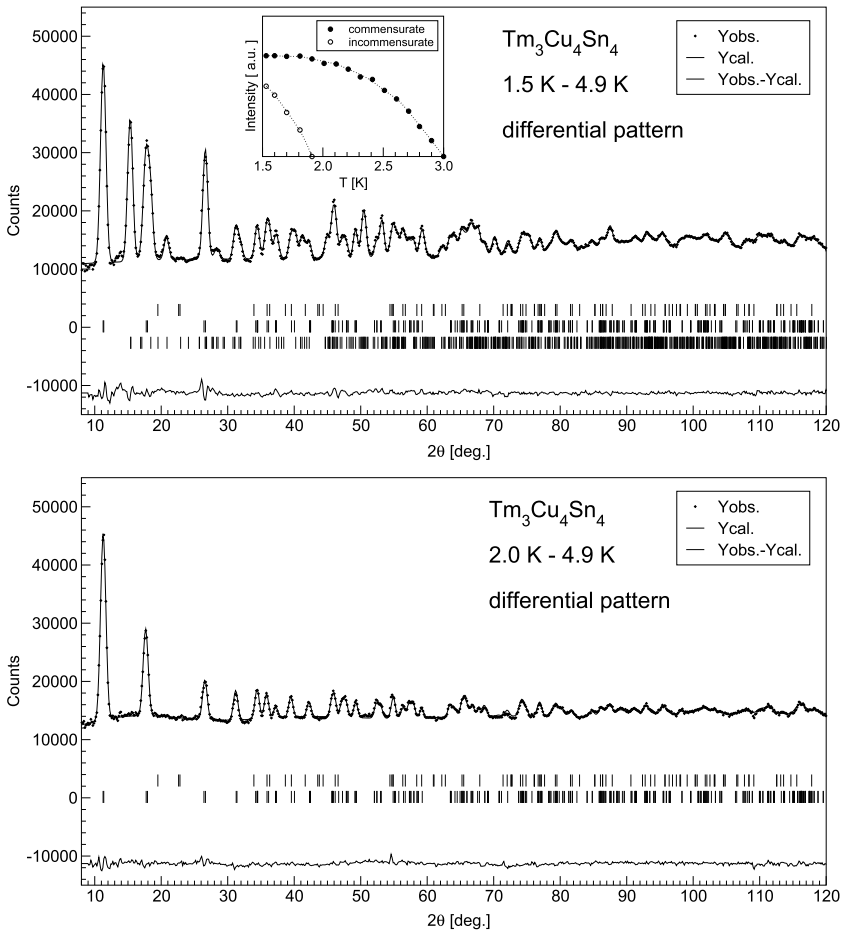

Figure 6. Magnetic contribution to neutron diffraction patterns of $Tm_3Cu_4Sn_4$ collected at 1.5 and 2.0 K together with Rietveld fit and difference plot. The differential patterns were extracted by subtracting the paramagnetic pattern taken at 4.9 K from the low-temperature ones. The upper row of vertical ticks indicates the positions of nuclear reflections (they are absent in differential pattern but were marked as a reference). The next row(s) indicates the positions of reflections originating from magnetic contributions. The inset shows the temperature dependence of magnetic reflections at $2\theta = 11.2°$ and $2\theta = 15.3°$ originating from commensurate and incommensurate magnetic order, respectively.

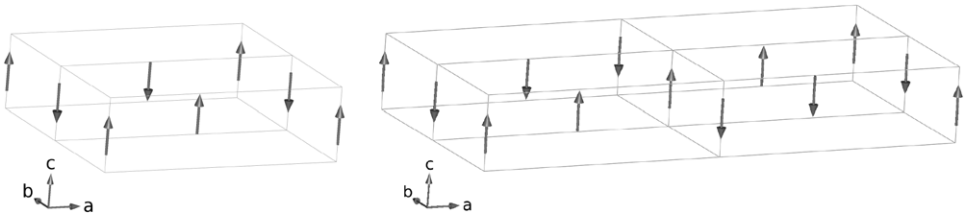

Figure 7. Commensurate components of $Tm_3Cu_4X_4$ (X = Ge, Sn) antiferromagnetic structures. For easier comparison the shape of an orthorhombic elementary unit cell is shown both for the germanide (on the left) and for the stannide (on the right).

and the 4i sublattice in monoclinic $Tm_3Cu_4Sn_4$ form an incommensurate antiferromagnetic structure (see figure 8). Remarkably, the crystal structure distortion in the stannide does not influence either the general formula of the propagation vector or the orientation of the thulium magnetic moments. The amplitude of modulation of the magnetic moment derived from the $Tm_3Cu_4Ge_4$ neutron diffraction pattern collected at 1.6 K equals 7.47 μ_B and exceeds the theoretical value of 7.0 μ_B. Thus one may expect some deviation from a pure sine function in equation (1), which can be expressed mathematically by adding higher harmonics. However, in the performed experiment no Bragg reflections originating from higher harmonics were observed, meaning that any possible deformation of the sine function was very small (probably only a top (bottom) of a sine was cut).

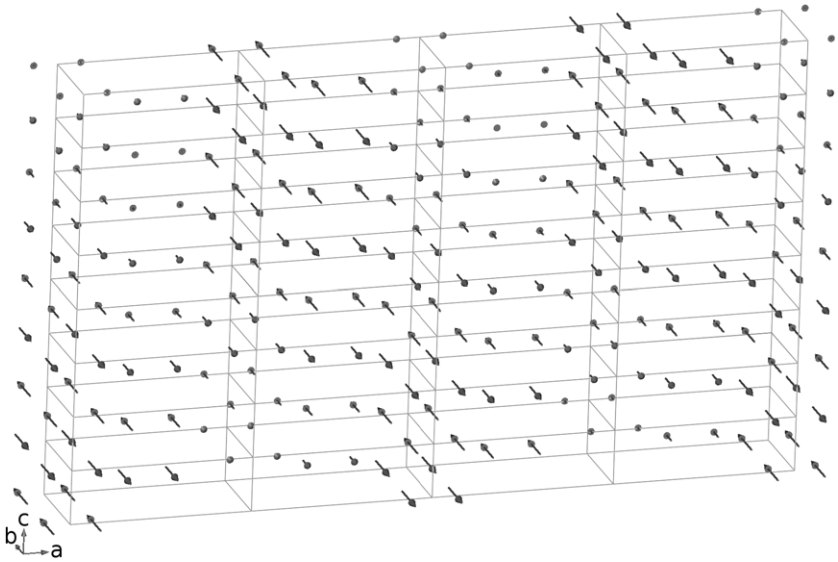

Figure 8. Incommensurate component of $Tm_3Cu_4X_4$ (X = Ge, Sn) antiferromagnetic structures drawn using an orthorhombic description of the crystal structure ($\vec{k} = [\frac{1}{4}, 0, k_z]$, with k_z being close to 0.5). It is not possible to draw a magnetic elementary unit cell because the structure is an incommensurate one. Nevertheless, the volume of several crystallographic unit cell was shown in order to give an idea of what the structure looks like.

Table 4. Refined parameters of $Tm_3Cu_4X_4$ (X = Ge, Sn) low-temperature antiferromagnetic structure consisting of both commensurate and incommensurate components together with residuals for profile and integrated magnetic intensities. The parameters were derived from the neutron diffraction patterns collected at 1.6 K and 1.5 K for germanide and stannide, respectively. SYM denotes crystal symmetry, PV—propagation vector, DMM—direction of magnetic moment, μ_A—amplitude of modulation and $\Delta\phi$—phase shift (see main text for details). In the case of the stannide, for better comparison with the germanide, both the monoclinic and orthorhombic descriptions are presented.

Compound	$Tm_3Cu_4Ge_4$	$Tm_3Cu_4Sn_4$	
T (K)	1.6	1.5	
SYM	Orthorhombic	Monoclinic	Orthorhombic[a]
	Commensurate component		
PV	$[0, \frac{1}{2}, 0]$	$[0, 0, \frac{1}{2}]$	$[\frac{1}{2}, \frac{1}{2}, 0]$
DMM	$\parallel c$	$\parallel b$	$\parallel c_{ortho}$
μ (μ_B)	6.65(14)	6.33(8)	6.23(13)
$R_{magnetic}$ (%)	8.23	4.43	7.25
	Incommensurate component		
PV	$[\frac{1}{4}, 0, 0.4911(1)]$	$[\frac{1}{4}, 0.4739(3), 0]$	$[\frac{1}{4}, 0, 0.4736(3)]$
DMM	$\parallel b$	$\parallel c$	$\parallel b_{ortho}$
μ_A (μ_B)	7.47(22)	6.95(10)	6.97(22)
$\Delta\phi$[b]	0.428(20)	0.411(12)	0.449(11)
$R_{magnetic}$ (%)	8.52	4.75	7.48
$R_{profile}$ (%)	2.90	1.63	2.96

[a] In fact the $Tm_3Cu_4Sn_4$ crystal structure shows a monoclinic distortion. The orthorhombic description was only used for easier comparison with $Tm_3Cu_4Ge_4$.
[b] Phase shift (in units of 2π) between magnetic moments on Tm_{21} (Tm_{22}) and those on Tm_{23} (Tm_{24}).

Observation of different magnetic ordering temperatures associated with different rare earth sublattices is a quite common phenomenon in the class of $R_3Cu_4X_4$ (X = Ge, Sn) intermetallics (cf the section 1). This feature likely arises because of different surroundings of rare earth ions located in the crystal unit cell at two inequivalent crystallographic sites.

Acknowledgments

This research project has been supported by the European Commission under the 6th Framework Programme through the Key Action: Strengthening the European Research Area, Research Infrastructures, Contract no: RII3-CT-2003-505925

Table 5. Comparison of magnetic ordering temperatures derived from different experimental data. M denotes magnetic susceptibility, C_p—specific heat, ER—electrical resistivity and ND—neutron diffraction.

Compound	$Tm_3Cu_4Ge_4$				$Tm_3Cu_4Sn_4$			
	M	C_p	ER	ND	M	C_p	ER	ND
T_N (K)	2.6	2.7	2.8	2.9	2.6	2.8	2.9	2.9
T_t (K)	2.0	2.1		2.3		1.7		1.8

(NMI3) and the Ministry of Science and Higher Education in Poland under Grant no. N N202 201039.

References

[1] Zaharko O, Keller L and Ritter C 2002 *J. Magn. Magn. Mater.* **253** 130

[2] Ryan D H, Cadogan J M, Voyer C J, Napoletano M, Riani P and Cranswick L M D 2010 *Mod. Phys. Lett.* B **24** 1

[3] Rieger W 1970 *Monatsh. Chem.* **101** 449

[4] Thirion F, Steinmetz J and Malaman B 1983 *Mater. Res. Bull.* **18** 1537

[5] Romaka L, Romaka V V and Davydov V 2008 *Chem. Met. Alloys* **1** 192

[6] Muñoz-Perez S, Cobas R, Susilo R A and Cadogan J M 2011 *J. Phys.: Conf. Ser.* **286** 012018

[7] Muñoz-Pérez S, Cobas R, Cadogan J M, Ryan D H, Lora-Serrano R, Figueira M J S and Yokaichiya F 2011 *Acta Crystallogr.* A **67** C247

[8] Dhar S K, Singh S, Bonville P, Mazumdar C, Manfrinetti P and Palenzon A 2002 *Physica* B **312/313** 846

[9] Singh S, Dhar S K, Manfrinetti P and Palenzona A 2002 *J. Magn. Magn. Mater.* **250** 190

[10] Wawrzyńska E, Hernández-Velasco J, Penc B and Szytuła A 2004 *J. Phys.: Condens. Matter* **16** 45

[11] Wawrzyńska E, Hernández-Velasco J, Penc B, Szytuła A and Tomala K 2004 *J. Phys.: Condens. Matter* **16** 7535

[12] Voyer C J, Ryan D H and Cadogan J M 2009 *J. Appl. Phys.* **105** 07D508

[13] Szytuła A, Wawrzyńska E, Penc B, Stüsser N and Zygmunt A 2003 *Physica* B **327** 167

[14] Szytuła A, Wawrzyńska E, Penc B, Stüsser N, Tomkowicz Z and Zygmunt A 2004 *J. Alloys Compounds* **367** 224

[15] Szytuła A, Jezierski A, Penc B, Wawrzyńska E and Zygmunt A 2006 *Phys. Status Solidi* b **243** 299

[16] Łątka K, Pacyna A W, Pöttgen R and Schappacher F M 2008 *Acta Phys. Pol.* A **114** 1501

[17] Voyer C J, Ryan D H, Napoletano M and Riani P 2007 *J. Phys.: Condens. Matter* **19** 156209

[18] Wawrzyńska E, Hernandez-Velasco J, Penc B, Szytuła A and Zygmunt A 2003 *J. Magn. Magn. Mater.* **264** 192

[19] Wawrzyńska E, Hernandez-Velasco J, Penc B, Sikora W, Szytuła A and Zygmunt A 2003 *J. Phys.: Condens. Matter* **15** 5279

[20] Cadogan J M, Ryan D H and Cranswick L M D 2010 *J. Phys.: Conf. Ser.* **200** 032009

[21] Gondek Ł, Szytuła A, Kaczorowski D, Szewczyk A, Gutowska M and Prokhnenko O 2007 *Intermetallics* **15** 583

[22] Ryan D H, Cadogan J M, Gagnon R and Swainson I P 2004 *J. Phys.: Condens. Matter* **16** 3183

[23] Rodriguez-Carvajal J 1993 *Physica* B **192** 55